A nanocomposite of copper(II) functionalized graphene and application for sensing sulfurated organophosphorus pesticides

By: Zhi Li, Heji Zhang, Xueping GE, Ying Liang, Xingcai An, Cunzhong Yang, Bin Fang, Haifen Xie and Jianjun Wei

Li Z., J. Zhang, et al and J. Wei, A Nanocomposite of copper (II) functionalized graphene and application for sensing sulfurated organophosphorus pesticides, New Journal of Chemistry, 2013, 37 (12), 3956 – 3963. DOI: 10.1039/C3NJ00528C

Abstract:

Reduced graphene oxide is modified with sulfanilic acid diazonium salt followed by copper(II) chelating to form a Cu complex nanocomposite. Characterization by Raman spectroscopy, FTIR and EDS, XPS, cyclic voltammetry demonstrates the successful functionalization of the graphene surfaces. Electrodes that are prepared by drop-casting the suspended nanocomposite solution on interdigitated electrodes (IDE) are tested for a novel pulsed amperometric detection of a series of sulfurated organophosphorus (SOP) pesticides, parathion, fenitrothion and malathion. A linear relationship of the pulsed amperometric current to the logarithmic value of concentration of the three SOPs is demonstrated with a R^2 value of ~0.95 at the S-OP concentration range of 1 ppb to 10^4 ppb. Negligible amperometric currents are observed in the control experiments using diethyl ethylphosphonate (DEEP) and dimethyl methyl phosphonate (DMMP), or S^{2-}, SO_3^{2-}, SO_4^{2-} ions, suggesting sensing specificity to sulfurated compounds.

Keywords: organophosphorus pesticides | graphene | organophosphorus compounds | electrochemical sensors

Article:

Introduction

As a two-dimensional carbon crystal with only one atom thickness, graphene has attracted enormous research activities due to the unique structure, mechanical and electronic properties as well as many other superior properties.[1–4] The unique properties make it highly attractive for numerous applications, especially in the areas of electronics,[5] energy,[6–10] sensors and biosensors.[11–15] As used for electrochemical sensors for organophosphorus pesticides (OPs), graphene has advantages of high surface area to increase the surface loading as a sorbent material, suitability for functionalization,

excellent conductivity and a small band gap for fast electron conduction.[16] It is reported that the planar geometry and "wrinkly" surface of graphene sheets, compared with the tube-shaped carbon nanotubes, could be due to closer contact with the surrounding matrix and stronger interactions with exotic molecules during functionalization.[17] Capitalising on these advantages, functionalization of graphene for both enzymatic[18]and nonenzymatic sensors to detect OP pesticides[19] or glucose[20,21] have been reported.

Organophosphorus compounds (OPs) have severe toxicity, broad-spectrum activity and low cost, making them popular as pesticides, insecticides and chemical warfare agents. These chemicals are considered extremely hazardous for human health, since they inhibit main metabolic pathways. OPs are severe neurotoxins, and inhibit acetylcholinesterase (AChe), the key enzyme in the transmission of nerve impulses.[22,23] The extensive use of these OPs has made them a serious threat to animal and human health, environment quality and food safety.[24,25] Accurate detection of OPs is critical for identification of potential health effects resulting from exposure to these toxic chemicals. In addition, OP detection is a necessary element of homeland security (to safeguard water resources and food supplies), as well as biodefense (force protection) applications. These applications are also driving the need for portable detection systems to provide reliable on-site monitoring.

While traditional assay techniques in analytical chemistry laboratories (GC-MS, HPLC-MS) offer high selectivity and sensitivity for OP identification and quantification, they require bulky, expensive instrumentation, complex and time-consuming sample preparation; are not adapted for *in situ* and real time detection, and require highly trained personnel.[26] For many years, great efforts have been made to develop low-cost, portable, easy to-use sensors or biosensors for detecting OP pesticides and their derivatives. Thanks to advances in miniaturization and microfabrication technology, great progress has been made in the development of sensitive and selective sensor, and biosensor devices for field-based and *in situ* applications, based mainly on electrochemical and optical techniques.[27,28] In the past few years, enzyme-based inhibition or non-inhibition electrochemical biosensors[29–31] for OP pesticides have attracted considerable interest because of their high sensitivity, low cost and readiness for miniaturization and integration with electrical systems.[11,32,33] However, the operational conditions are mostly limited by the stability of enzymes. To address this challenge, researchers have sought stable, nonenzymatic, electrochemical sensors for sensitive detection of OP pesticides. A method combining solid phase extraction with stripping voltammetric analysis for pesticide detection has been reported,[19,34] however, it is challenging to construct a high-performance solid-phase extraction platform for sensitive and selective detection of OPs. Therefore, an alternative rapid, sensitive, reliable and field deployable enzymeless electrochemical sensor is desirable for the detection of OP residues.

In this paper, a unique enzymeless amperometric electrode based-on copper-chelating functionalized graphene is reported for rapid, ultrasensitive detection of sulfurated organophosphorus (SOP) pesticides which are among the most widely used pesticides in agriculture due to their high effectiveness for insect extermination. The reduced graphene oxide is sulfonated first then reacts with Cu(II) to form a metal ion chelated graphene nanocomposite which is drop-casted to an interdigitated electrode (IDE 5 mm × 5 mm). Due to the specific interaction of SOPs to the Cu(II) graphene complex[35,36] at the reduction potential (applied negative voltage, −0.4 V *vs.* Ag/AgCl), a rapid, pulsed amperometric response is observed when an SOP pesticide accesses the nanocomposite modified electrode through ligand binding interactions.[37] No significant amperometric current is observed upon addition of SOPs when the voltage is set at the oxidation potential (applied positive voltage, 0.1

V *vs.*Ag/AgCl), suggesting a dependence on the redox status of copper ions in the nanocomposite electrode.

Experimental

Materials

Graphene oxide used in this work was prepared *via* a modified Hummers redox method.[38] High purity graphite was obtained from Qingdao graphite Co. Sulfurated organophosphorus pesticides including fenitrothion, malathion and parathion were purchased from Beijing YiHua sgs-cstc Technology Co. Ltd. The pesticides were prepared in 0.1 M phosphate buffer solution (pH 7) used in concentrations of 1 ppb, 10 ppb, 10^2 ppb, 10^3 ppb and 10^4 ppb. Organophosphorus compounds, diethyl ethylphosphonate (DEEP 98%) and dimethyl methyl phosphonate (DMMP 97%), were purchased from Sigma-Aldrich. All other chemicals were obtained of analytical grade and were used as received, unless otherwise noted. Distilled water (18 MΩ) was used for all aqueous solutions. 0.1 M phosphate buffer was prepared using Na_2HPO_4 and NaH_2PO_4. Sulfanilic acid diazonium salt was prepared by 4-aminobenzene sulfonic acid, $NaNO_2$, NaOH and HCl.

Functionalization of graphene

Sulfonated graphene was prepared according to a previously reported procedure.[39] Firstly, the GO was pre-reduced by $NaBH_4$ at 80 °C for 2 h followed by post-reducing with hydrazine hydrate at 100 °C for 24 h. Then the reduced graphene oxide (RGO) was purified by dialysis with distilled water until the pH exchanged water was about 7.0. Secondly, RGO was sulfonated by excess sulfanilic acid diazonium salt for 2 h in an ice bath while the pH of the solution was maintained about 10. The obtained sulfonated graphene (SG) was further purified by dialysis with distilled water until the exchange water became colorless and the pH turned to 6.5. A certain amount of $CuCl_2{\cdot}2H_2O$ was added to the SG solution and followed by supersonic vibration for 30 min. After that, the mixed liquor was centrifuged at 10 000 rpm, supernatant (superfluous copper(II) salt solution) was discarded and the deposit was collected and washed by distilled water followed by centrifuging at 10 000 rpm. This process was repeated until the supernatant was free of copper(II) ions. Finally the deposit was dispersed into distilled water by ultrasonication to give a certain concentration of suspended sulfonated graphene with copper(II) ions complexation (SG-Cu(II)).

Characterization

AFM images of GO on a freshly cleaved mica surface were obtained by NanoScope IIIa MultiMode atomic force microscopy (Veeco) in tapping mode. A droplet of GO or RGO dispersion was cast onto a freshly cleaved mica surface. The sample was kept at room temperature overnight for water to evaporate completely. Fourier transform infrared (FTIR, Nicolet 6700, UK) and Raman spectroscopy (RM, 514 nm, Renishaw UK) were used to characterize the surface structure of GO, reduced graphene oxide (RGO) and sulfonated graphene (SG). Surface element analysis of GO, SG and SG-Cu was performed by Energy disperse spectroscopy (EDS, QUANTAX 40, Hitachi Co, Japan). The Castaing's approximation was used for semiquantitative analysis of the surface elements. X-ray photoelectron spectroscopy (XPS) was used to measure the elemental composition of the nanocomposite electrode, specifically to measure the copper element before and after the

electrochemical detection of a SOP. The samples were tested by Al Kα (1486.6 eV) mono excitation source and scanned by wide mode and narrow mode respectively under 150 W using the instrument AXIS Ultra^{DLD} (Shimadzu-kratos Co. LTD).

Electrode preparation and electrochemical measurements

The working electrode was prepared using the SG-Cu(II) suspension, which is similar to a drop-casting process using the multi-walled carbon nanotube suspension reported recently.[40] Briefly, an aliquot of 50 µl of uniformly suspended SG-Cu(II) water solution was drop casted at the surface of the IDE area (25 mm^2). The electrode was cured in a drying oven at 50 °C for 30 min. For control studies, the SG electrodes were made using suspended SG solution by similar means.

Results and discussion

Characterization of GO and functionalized graphene

AFM was used for examining the morphology and thickness of the GO. Fig. 1 (top panel) shows the AFM image of GO. The section analysis of the AFM image of GO indicates that the average thickness of the GO sheet is around 0.9 nm which is 'thicker' than the well-known thickness of the atomically flat sheet (0.34 nm), due to the presence of covalently bound oxygen containing groups, which is a feature of a fully exfoliated GO sheet.[4,41] The AFM studies suggest that the dispersions of GO comprised isolated graphitic sheets.

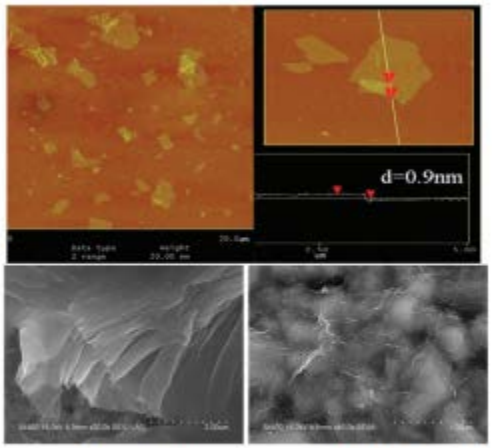

Fig. 1 AFM micrograph and thickness analysis of GO (upper panel) and SEM images (lower panel) of GO and after sulfonation-Cu functionalization, SG-Cu complex.

Morphology characterization of GO and after functionalization with sulfonation-Cu complex after drop-casting was also conducted by scanning electron microscopy (SEM). Fig. 1 (lower panel) demonstrates SEM images of the typical morphology of GO and SG-Cu. The image of GO clearly illustrates flake-like shapes. The surface morphology of the SG-Cu composite displays a "wrinkly" structure with stacked distribution, indicating randomly aggregated and some extended folded sheets. This structure provides a good contact for interaction with exotic molecules for sensitive detection.

Functionalization of the RGO with sulfonation was characterized and confirmed with Raman spectroscopy, FTIR. The bands at 1580 and 1350 cm^{-1} in the Raman spectra (Fig. 2) are assigned to the G band and D band associated with the vibration of $sp^2$and sp^3 carbon atoms, respectively. The intensity ratio of the D band to the G band decreases from 0.96 (for graphene oxide) to 0.86 (for post-reduced graphene) after chemical reduction, suggesting a decrease of dangling bonds (unsatisfied valences) of graphene surface,[42] namely fewer defects of the graphene structures. The defects in GO are mainly caused from the bonds of C–H or COO or C=O in hydroxyl, carboxyl, carbonyl, and epoxide groups. The ratio increases from 0.86 (for post-reduced graphene) to 0.92 (for sulfonated graphene) after sulfonation, which is expected because more defects were induced by the sulfonation functionalization. Fig. 3 displays the FTIR spectra of GO and SG. A significant band at 1736 cm^{-1} of GO represents the oxidation groups on the GO surface.

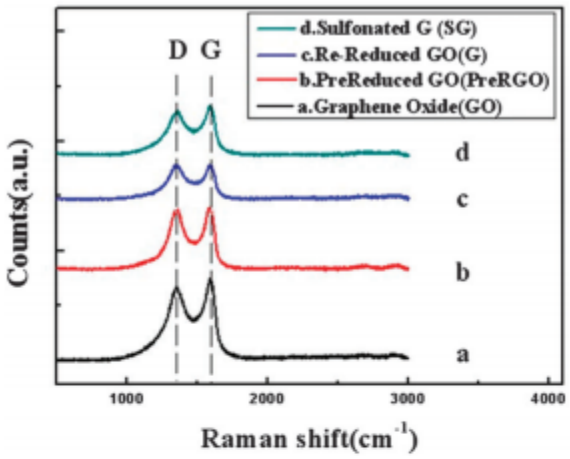

Fig. 2 Raman spectrum of GO (a), Pre-RGO (b), RE-Reduced GO (c) and SG (d).

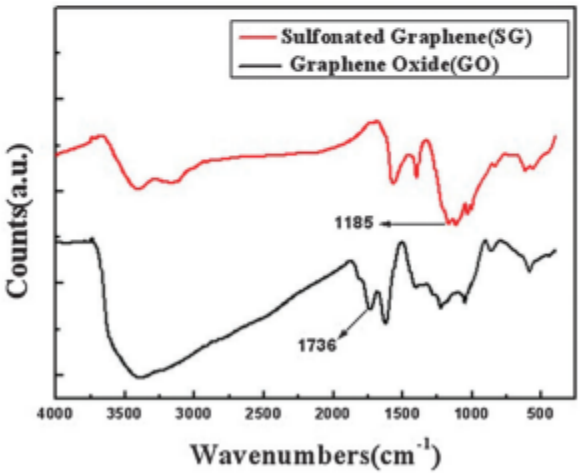

Fig. 3 FTIR spectroscopy of GO and SG.

The increase of the band at 1185 cm^{-1} and the decrease of the band at 1736 cm^{-1} at the SG surface suggest the existence of sulfonic acid groups at the oxidation groups. Both the Raman and FITR data clearly demonstrate the successful modification of sulfonation at the oxidation groups of the GO.

In order to further investigate the Cu(II) functionalization to the sulfonated graphene, elemental analysis was performed using EDS and XPS. The area of a sample used for EDS analysis is shown as a SEM image in Fig. S1 (ESI†). Fig. 4 shows the EDS spectra of surface chemical elements of GO, SG and SG-Cu(II), respectively. At the GO surfaces, two strong X-ray peaks between 0 to 1 eV represent the carbon and oxygen, while no X-ray spectrum corresponding to sulfur (S) or copper elements is observed. From the X-ray spectrum of SG, an X-ray response at 2.3 eV appears, representing the existence of sulfur element. The X-ray response corresponding to copper element is only displayed in the spectra of the SG-Cu surface. Further semiquantitative analysis was made according to Castaing's approximation. Table S1 (ESI†) presents the estimated results of the elemental percentages of the three samples. The clear evidence of the chemical composition of the SG-Cu surfaces confirms successful modification of GO copper ion functionalization.

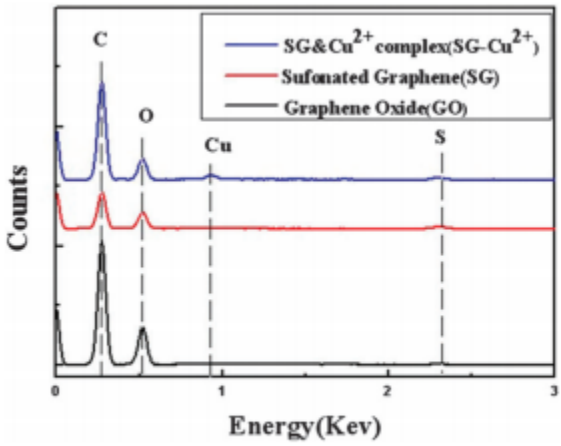

Fig. 4 EDS spectra of surface atom (C, O, Cu and S) analysis for GO, SG and SG-Cu^{2+}.

The XPS spectra of the SG-Cu(II) complex before and after the detection of parathion were measured. Fig. 5 (full spectrum see Fig. S6, ESI†) displays the representative spectra of the copper (Cu2P) element. During the measurement no electrochemical voltage was applied to the complex and the sample was set at the equilibrium state. The spectra have a major peak at ~935 eV and a satellite characteristic signal of Cu(II) at peak ~944 eV, indicating copper at the electrode before and after the parathion detection is dominated with Cu(II) complex.[43] The binding of SOP to the complex has an insignificant impact on the status of the Cu complex.

† Electronic supplementary information (ESI) available: Including SEM 60 image of nanocomposite for EDS and elementary analysis of EDS, a full spectra of XPS. Figures of amperometric responses at positively applied voltage, and figures of amperometric responses of inorganic ions containing sulfur. See DOI: 10.1039/c3nj00528c

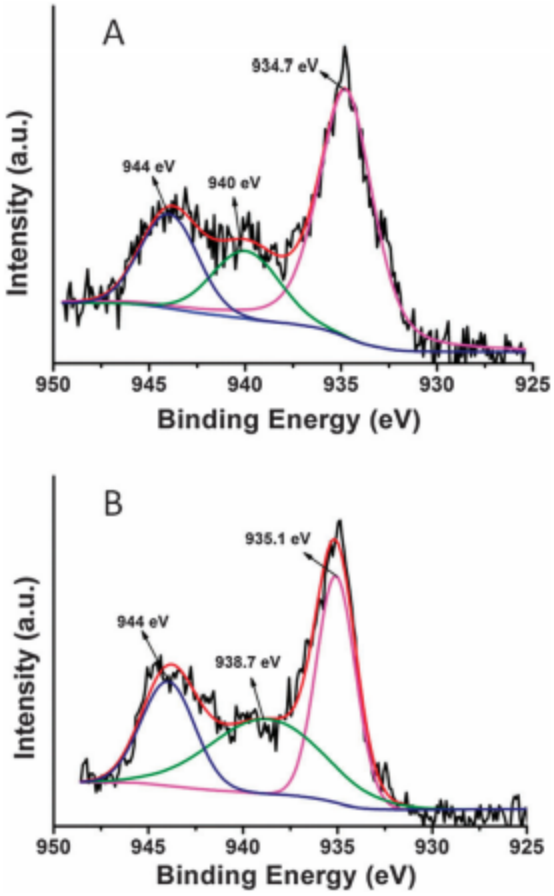

Fig. 5 XPS spectra of the copper complex at the electrode surface before (A) and after (B) detection of parathion.

Electrochemistry and detection of SOPs

Electrochemical characterization of the modified electrodes. Cyclic voltammetric response of the SG and SG-Cu modified electrodes in 0.1 M PBS (pH 7) are obtained and shown in Fig. 6. The SG modified electrode is not electrochemically active in the potential window from −1.0 to 1.0 V *vs.* Ag/AgCl. After Cu(II) functionalization, a pair of redox peaks are observed. The redox peaks can be attributed to the electron transfer reaction between the copper ions to the graphene electrode where copper ions are intercalated in the graphene nanocomposite through affinity interaction between the negatively charged sulfonation functional group and copper ions.

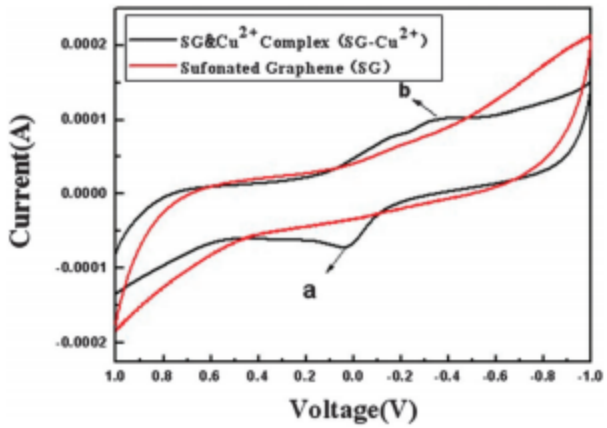

Fig. 6 Cyclic voltammograms (CVs) of SG and SG-Cu(II) electrodes respectively.

Detection of SOPs. Three widely used SOPs, parathion, fenitrothion and, malathion, were chosen to demonstrate the sensing application by using the SG-Cu(II) modified electrode. Typical amperometric current–time responses of the three SOPs are shown in Fig. 7. The immediate amperometric current responses (a few seconds) upon injection of SOPs in the electrochemical cell are observed. When different SG-Cu(II) electrodes are used, the amperometric responses are similar, though a variability (~±10%) of absolute current value between different electrodes are observed, which may be caused by the different amounts of Cu(II) immobilized at the individual electrodes.

As a comparison, SG deposited electrodes were used to investigate the role of the copper ion complex in the sensor. Fig. 8a illustrates a typical amperometric current response of a SG electrode to the addition of different concentrations of parathion; Fig. 8b presents a comparison of the current responses from SGCu and SG electrodes, respectively. The average current response of SG electrodes is less than 5% of SG-Cu electrode. Moreover, the amplitude of the current does not increase with the concentration increase of parathion for SG modified electrodes. This experiment suggests the key role of Cu(II) in the SG-Cu electrode to generate the amperometric current for SOP detection, rather than the physical absorption and/or desorption ability of graphene complex *via* van der Waals attractive forces.[40]

The pulsed amperometric response of SG-Cu electrode upon addition of SOPs is different from a regular amperometric sensor. In addition, the amperometric response is voltage dependent and occurs at negatively applied voltage; no significant amperometric current is observed at positively applied voltage 0.1 V *vs.* Ag/AgCl (Fig. S2A–C, ESI†), suggesting the importance of the status of Cu ions in the complex. We hypothesize that the ligand binding reaction between the Cu ions to SOP induces the amperometric responses. Namely, during the amperometric experiments, at the applied voltage −0.4 V *vs.* Ag/AgCl, Cu(II) in the electrode is reduced to Cu(I). The Cu(I) has an empty orbital 4s, when an SOP is added in the solution, a ligand binding interaction occurs immediately due to the two unshared pairs of electrons (as donor) of the sulfur element in the SOP. It is plausible that the pulsed electrical current is triggered immediately because of the formation of the ligand Cu complex.[44–47] The hypothesized mechanism of the SG-Cu(II) electrode for SOP detection is most likely a binding reaction induced electronic perturbation following inner sphere charge transfer in the copper–SOP complex, thus a pulsed amperometric response is expected.

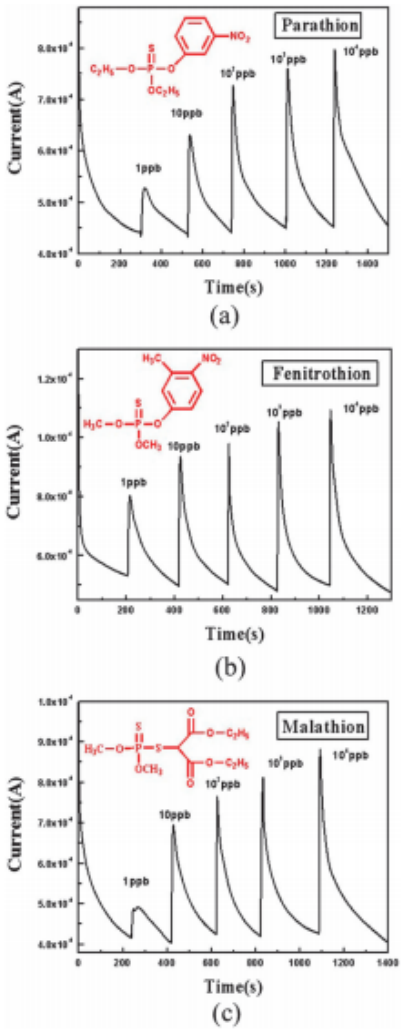

Fig. 7 Typical amperometric current–time curve responses with different concentrations from 1 ppb to 10^4 ppb of parathion (a), fenitrothion (b) and malathion (c), respectively by SG-Cu(II) modified electrodes at −0.4 V *vs.* Ag/AgCl.

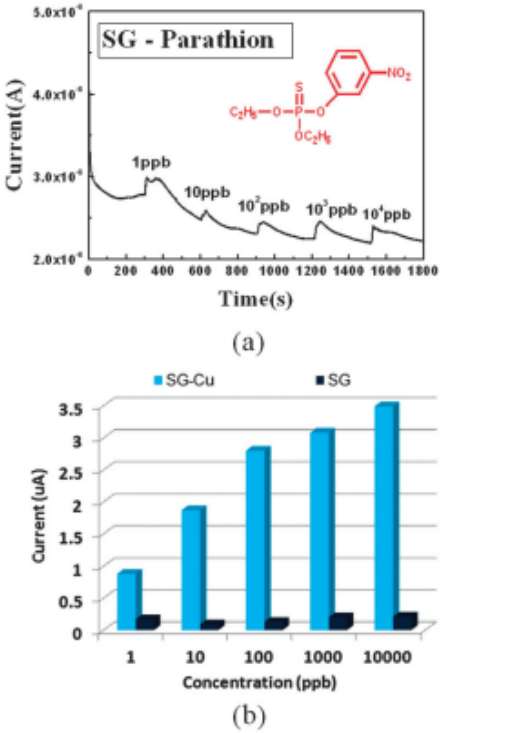

Fig. 8 (a) Amperometric response of parathion to the SG-deposited electrode, (b) a comparison of amperometric current amplitude of SG Cu(II) *vs.* SG electrodes.

Recently, Luo *et al.*[20] reported the use of CuO nanocubes–graphene nanocomposite for glucose sensing based on the strong oxidizing property of Cu(III) at an applied positive voltage. In our case, a negative voltage applied to the SG-Cu(II) electrode is used, it is not an oxidative process for SOP detection. According to the above described binding induced charge exchange mechanism, it is expected that the copper remains in the 2+ state in the complex when negative voltage is released (no external applied voltage), thus the states of the copper ions should have no significant change before and after electrochemical detection. This is in agreement with the XPS study indicated in Fig. 5.

For a quick amperometric reaction, the amplitude of the amperometric current follows the Butler–Volmer equation, $i = AFj$, (where A is the area of the electrode, F is the Faraday constant, and j is the flux of the SOP reaching the electrode), and is proportional to the concentration of the SOP injected in the solution. However, in this case, it is expected that the amplitude of the pulsed current should be limited by the kinetics of the ligand binding reaction; the relationship of the signal (current) to the analyte concentration follows the law of an affinity sensor. Hence, a linear relationship of the

amplitude of the amperometric current to the logarithmic value of concentration of the added SOP is expected[48] (*vide infra*). The amperometric curve restores to its baseline after flowing with PBS and the sensor is regenerated. The SG-Cu sensor is ready for the next concentration detection, suggesting a reversible affinity interaction and a repeatedly renewable affinity – sensing interface for SOPs, similar to a previously reported electrochemical affinity sensor.[49]

The repeatability and reusability of the sensor were investigated using an SG-Cu electrode for monitoring a sequence injection of the same concentration (100 ppb) of an SOP, fenitrothion. The amperometric response is shown in Fig. 9. The current pulses correspond to the addition of fenitrothion at sufficient time intervals (~300 s) between each injection for the amperometric curve to return to the baseline. The amplitude of the three pulse currents display insignificant changes (decrease < 5%), indicating a good repeatability of the SG-Cu electrode after regeneration. More research to gain an insight into the SG-Cu electrode reaction and interaction mechanism with SOPs is underway and will be published elsewhere.

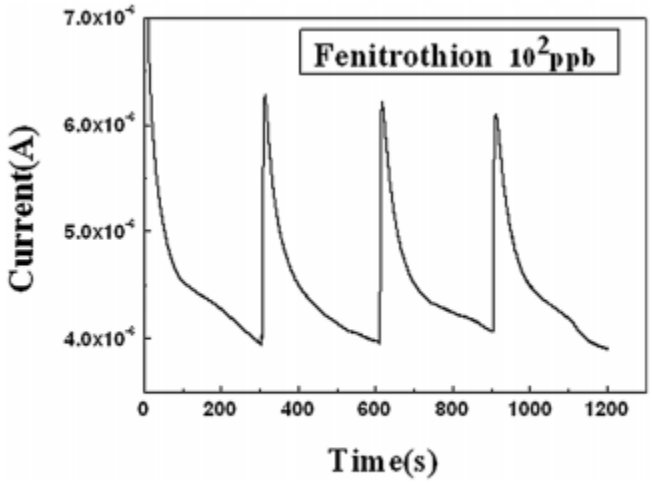

Fig. 9 Amperometric response to sequential addition of the same concentration of fenitrothion.

Selectivity: a comparison study with OP compound and sulphur-containing ions

In order to investigate the ability to differentiate SOPs from general OP compounds, DEEP and DMMP were chosen to measure the amperometric responses from the SG-Cu electrodes. Fig. 10 displays the response curve of current *vs.* time with the addition of a variety of concentrations of DEEP and DMMP, respectively. The small pulsed currents arise from the physical interactions with the graphene complex surfaces when adding the OPs to the solution.

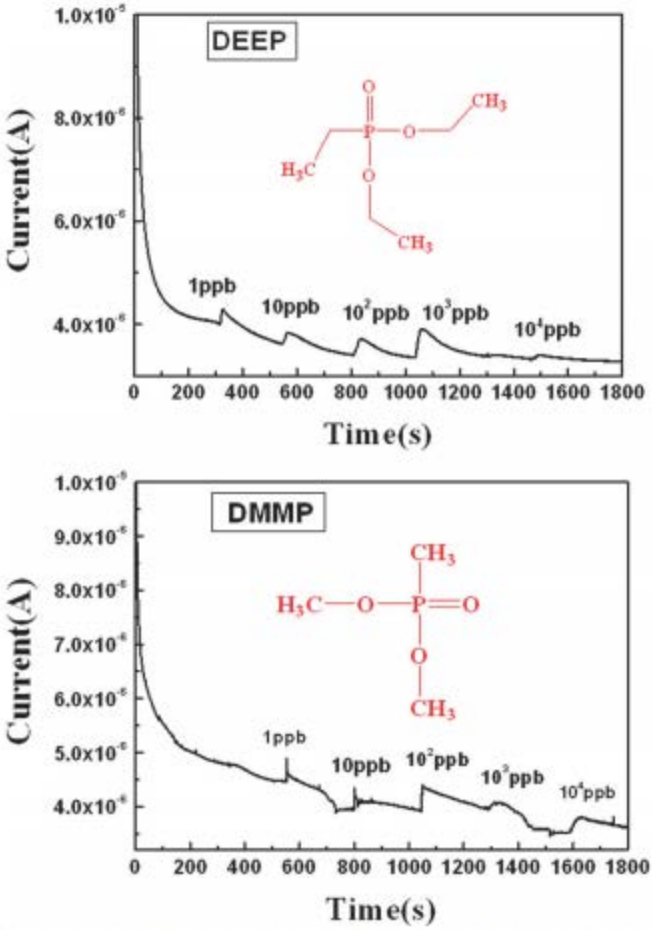

Fig. 10 Amperometric responses of SG-Cu electrodes with addition of DEEP and DMMP, respectively.

The correlation of the amperometric current to the measured SOPs and OPs are summarized in Fig. 11. A linear relationship of the amplitude of amperometric current to the logarithmic value of concentration of the detected SOPs is demonstrated with an R^2 value of about 0.95 ± 0.2 at the range of 1 ppb to 10^4 ppb, which agrees with analysis of the ligand binding reaction mechanism. The lowest concentration reported here is 1 ppb with a signal-to-noise ratio > 50, highly sensitive and comparable to most enzymatic OP sensors reported in the literature. As a contrast, the amperometric current resulting from the addition of DEEP or DMMP is negligible. It is also evident for the sulfur–copper binding interactions as well.

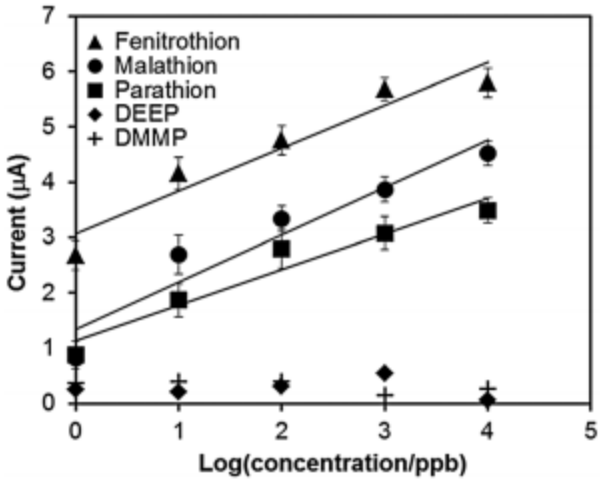

Fig. 11 Linear relationship between amperometric response and the logarithmic value of the concentration of SOPs from 1 ppb to 104 ppb at the SG Cu electrode; The negligible current responses from OPs indicate the selectivity for SOP detection.

We further investigated possible interference caused by inorganic sulfur-containing ions, such as (S^{2-}, $-SO_3^{2-}$, SO_4^{2-}). Amperometric responses of the SG-Cu modified electrode with addition of these ions were measured and the results are shown in Fig. S3–S5 (ESI†). The amplitude of the current is less than 2% of that generated from SOP at the same concentrations. In addition, the amperometric currents do not change along with the increased concentrations of the ions, suggesting a weak physical interaction from the addition of the sulfur-containing ions.

The amperometric responses of the three SOPs are similar because of their structural similarity of the sulfur element to the phosphate center. While the SG-Cu sensor may not be able to distinguish the SOP individually, this research, to the best of our knowledge, reports for the first time the ability to differentiate SOPs from generic OP compounds using a very simple enzymeless, graphene-based nanocomposite electrode as a novel electrochemical detection of a class of commonly used pesticides. The high electrical conductivity of graphene contributes to the fast response of electron transfer between the copper ions to the solid IDE and the high detection sensitivity because of the large surface area for contact. The preparation of graphene–copper complex is straightforward. The S-OP sensor device is easy to fabricate and operate. The experimental results indicate a high sensitivity and ultra-low amounts of SOPs are detectable.

Conclusions

In this paper, a novel, simple, enzymeless, amperometric sensor based on copper(II) chelating functionalized graphene nanocomposite has been successfully demonstrated for differentiating detection of SOP pesticides from generic OP agents. The copper ion functionalization of graphene nanocomposite is well characterized and shows a good stability for the sensor application. The ligand-interaction triggered amperometric response of the copper complex allows injection flow detection mode with the capability of self-regeneration and excellent repeatability. The sensor has demonstrated rapid (3–5 s), ultrasensitive responses to three selected SOP pesticides at concentrations from 1 ppb to 10^4 ppb. Moreover, interference from generic OPs and inorganic sulfur containing ions (S^{2-}, $-SO_3^{2-}$, SO_4^{2-}) is investigated and negligible. This work provides a new methodology and a generic platform

which may potentially be developed to a miniaturized, portable electrochemical analytical device for monitoring residues of SOP pesticides, and other sulfurated compounds in water or other environmental samples.

Acknowledgements

This work was financially supported by the National Natural Science Foundation of China (No. 51103039). J. Wei thanks support from the JSNN.

References

1. K. S. Novoselov, V. I. Falko, L. Colombo, P. R. Gellert, M. G. Schwab and K. Kim, *Nature*, 2012, **490**, 192–200
2. K. Geim and K. S. Novoselov, *Nat. Mater.*, 2007, **6**, 183–191
3. W. Choi, I. Lahiri, R. Seelaboyina and Y. S. Kang, *Crit. Rev. Solid State Mater. Sci.*, 2010, **35**, 52–71
4. Y. Zhu, S. Murali, W. Cai, X. Li, J. W. Suk, J. R. Potts and R. S. Ruoff, *Adv. Mater.*, 2010, **22**, 3906–3924
5. N. O. Weiss, H. Zhou, L. Liao, Y. Liu, S. Jiang, Y. Huang and X. Duan, *Adv. Mater.*, 2012, **24**, 5782–5825
6. L. Kavan, J. H. Yum and M. Grätzel, *ACS Nano*, 2011, **5**, 165–172
7. X.-Y. Peng, X.-X. Liu, D. Diamond and K. T. Lau, *Carbon*, 2011, **49**, 3488–3496
8. X. Wang, L. Zhi and K. Mullen, *Nano Lett.*, 2008, **8**, 323–327
9. Y. Zhu, S. Murali, M. D. Stoller, K. J. Ganesh, W. Cai, P. J. Ferreira, A. Pirkle, R. M. Wallace, K. A. Cychosz, M. Thommes, D. Su, E. A. Stach and R. S. Ruoff, *Science*, 2011, **332**, 1537–1541
10. E. Pollak, B. Geng, K.-J. Jeon, I. T. Lucas, T. J. Richardson, F. Wang and R. Kostecki, *Nano Lett.*, 2010, **10**, 3386–3388
11. Y. Shao, J. Wang, H. Wu, J. Liu, I. A. Aksay and Y. Lin, *Electroanalysis*, 2010, **22**, 1027–1036
12. R. Arsat, M. Breedon, M. Shafiei, P. G. Spizziri, S. Gilje, R. B. Kaner, K. Kalantar-zadeh and W. Wlodarski, *Chem. Phys. Lett.*, 2009, **467**, 344–347
13. G. Ko, H. Y. Kim, J. Ahn, Y. M. Park, K. Y. Lee and J. Kim, *Curr. Appl. Phys.*, 2010, **10**, 1002–1004
14. J. T. Robinson, F. K. Perkins, E. S. Snow, Z. Wei and P. E. Sheehan, *Nano Lett.*, 2008, **8**, 3137–3140
15. F. Schedin, A. K. Geim, S. V. Morozov, E. W. Hill, P. Blake, M. I. Katsnelson and K. S. Novoselov, *Nat. Mater.*, 2007, **6**, 652–655
16. S. Stankovich, D. A. Dikin, G. H. Dommett, K. M. Kohlhaas, E. J. Zimney, E. A. Stach, R. D. Piner, S. T. Nguyen and R. S. Ruoff,*Nature*, 2006, **442**, 282–286
17. M. A. Rafiee, J. Rafiee, Z. Wang, H. Song, Z.-Z. Yu and N. Koratkar, *ACS Nano*, 2009, **3**, 3884–3890
18. T. Liu, H. Su, X. Qu, P. Ju, L. Cui and S. Ai, *Sens. Actuators, B*, 2011, **160**, 1255–1261
19. J. Gong, X. Miao, T. Zhou and L. Zhang, *Talanta*, 2011, **85**, 1344–1349
20. L. Luo, L. Zhu and Z. Wang, *Bioelectrochemistry*, 2012, **88**, 156–163
21. J. Luo, S. Jiang, H. Zhang, J. Jiang and X. Liu, *Anal. Chim. Acta*, 2012, **709**, 47–53
22. L. D. Karalliedde, P. Edwards and T. C. Marrs, *Food Chem. Toxicol.*, 2003, **41**, 1–13
23. N. Motoyama and W. C. Dauterman, *J. Agric. Food Chem.*, 1974, **22**, 350–356

24. B. Heuer, Y. Birk and B. Yaron, *J. Agric. Food Chem.*, 1976, **24**, 611–614
25. D. Racke Kenneth, in *Environmental Fate and Effects of Pesticides*, American Chemical Society, 2003, vol. 853, pp. 96–123
26. L. Alder, K. Greulich, G. Kempe and B. Vieth, *Mass Spectrom. Rev.*, 2006, **25**, 838–865
27. E. J. Llorent-Martínez, P. Ortega-Barrales, M. L. Fernández-de Córdova and A. Ruiz-Medina, *Anal. Chim. Acta*, 2011, **684**, 30–39
28. G. Aragay, F. Pino and A. Merkoçi, *Chem. Rev.*, 2012, **112**, 5317–5338
29. Chen, D. Du and Y. Lin, *Environ. Sci. Technol.*, 2012, **46**, 1828–1833
30. B. Dzantiev, A. V. Zherdev, O. G. Romanenko and J. N. Trubaceva, in *Immunochemical Technology for Environmental Applications*, American Chemical Society, 1997, vol. 657, pp. 87–96
31. K. M. Mitchell, *Anal. Chem.*, 2004, **76**, 1098–1106
32. D. W. Kimmel, G. LeBlanc, M. E. Meschievitz and D. E. Cliffel, *Anal. Chem.*, 2012, **84**, 685–707
33. Y. Lin, J. Wang, G. Liu and C. Timchalk, in *Nanoscience and Nanotechnology for Chemical and Biological Defense*, American Chemical Society, 2009, vol. 1016, pp. 85–98
34. G. Liu and Y. Lin, *Anal. Chem.*, 2005, **77**, 5894–5901
35. Dannenberg and S. O. Pehkonen, *J. Agric. Food Chem.*, 1998, **46**, 325–334
36. M. R. Seger and G. E. Maciel, *Environ. Sci. Technol.*, 2006, **40**, 552–558
37. H. Choi, K. Yang, J. K. Park and I. S. Koo, *Bull. Korean Chem. Soc.*, 2010, **31**, 1339–1342
38. D. C. Marcano, D. V. Kosynkin, J. M. Berlin, A. Sinitskii, Z. Sun, A. Slesarev, L. B. Alemany, W. Lu and J. M. Tour, *ACS Nano*, 2010, **4**, 4806–4814
39. G. Zhao, L. Jiang, Y. He, J. Li, H. Dong, X. Wang and W. Hu, *Adv. Mater.*, 2011, **23**, 3959–3963
40. H. Xie, C. Sheng, X. Chen, X. Wang, Z. Li and J. Zhou, *Sens. Actuators, B*, 2012, **168**, 34–38
41. K. P. Loh, Q. L. Bao, G. Eda and M. Chhowalla, *Nat. Chem.*, 2010, **2**, 1015–1024
42. S. Stankovich, D. A. Dikin, R. D. Piner, K. A. Kohlhaas, A. Kleinhammes, Y. Jia, Y. Wu, S. T. Nguyen and R. S. Ruoff, *Carbon*, 2007, **45**, 1558–1565
43. M. C. Biesinger, L. W. M. Lau, A. R. Gerson and R. S. C. Smart, *Appl. Surf. Sci.*, 2010, **257**, 887–898
44. R. V. Parish, Z. Salehi and R. G. Pritchard, *Angew. Chem., Int. Ed. Engl.*, 1997, **36**, 251–253
45. L. M. Brines, J. Shearer, J. K. Fender, D. Schweitzer, S. C. Shoner, D. Barnhart, W. Kaminsky, S. Lovell and J. A. Kovacs, *Inorg. Chem.*, 2007, **46**, 9267–9277
46. S. Han, X.-Y. Liu, Z.-F. Cai, Z.-P. Wu, W.-T. Yin, X.-D. Xie, J.-R. Zhou, L.-M. Yang and C.-L. Ni, *Inorg. Chem. Commun.*, 2012,**24**, 91–94
47. Y.-Y. Yin, X.-C. Cao, P. Cheng and J.-G. Ma, *Inorg. Chem. Commun.*, 2012, **24**, 7–10
48. H. C. Yoon, M.-Y. Hong and H.-S. Kim, *Anal. Biochem.*, 2000, **282**, 121–128
49. H. C. Yoon, D. Lee and H.-S. Kim, *Anal. Chim. Acta*, 2002, **456**, 209–218